ELSEVIER

Journal of Membrane Science 188 (2001) 115–128

journal of MEMBRANE SCIENCE

www.elsevier.nl/locate/memsci

Influence of membrane surface properties on initial rate of colloidal fouling of reverse osmosis and nanofiltration membranes

Eric M. Vrijenhoek [a], Seungkwan Hong [b], Menachem Elimelech [a,*]

[a] *Department of Chemical Engineering, Environmental Engineering Program, Yale University, P.O. Box 208286, New Haven, CT 06520-8286, USA*

[b] *Civil and Environmental Engineering Department, University of Central Florida, P.O. Box 162450, Orlando, FL 32816-2450, USA*

Received 28 November 2000; received in revised form 6 February 2001; accepted 9 February 2001

Abstract

Recent studies have shown that membrane surface morphology and structure influence permeability, rejection, and colloidal fouling behavior of reverse osmosis (RO) and nanofiltration (NF) membranes. This investigation attempts to identify the most influential membrane properties governing colloidal fouling rate of RO/NF membranes. Four aromatic polyamide thin-film composite membranes were characterized for physical surface morphology, surface chemical properties, surface zeta potential, and specific surface chemical structure. Membrane fouling data obtained in a laboratory-scale crossflow filtration unit were correlated to the measured membrane surface properties. Results show that colloidal fouling of RO and NF membranes is nearly perfectly correlated with membrane surface roughness, regardless of physical and chemical operating conditions. It is further demonstrated that atomic force microscope (AFM) images of fouled membranes yield valuable insights into the mechanisms governing colloidal fouling. At the initial stages of fouling, AFM images clearly show that more particles are deposited on rough membranes than on smooth membranes. Particles preferentially accumulate in the "valleys" of rough membranes, resulting in "valley clogging" which causes more severe flux decline than in smooth membranes.

Keywords: AFM; Fouling; Flux decline; Membrane surface roughness; Colloidal fouling; Nanofiltration; Membrane surface properties

1. Introduction

Successful utilization of membrane technology has been greatly limited by membrane fouling. Fouling increases operation and maintenance costs by deteriorating membrane performance and ultimately shortening membrane life. Numerous studies in recent years have investigated the causes and control of membrane fouling, and substantial progress has been made. However, in many applications colloidal fouling of membranes continues to be a serious problem, thus pointing out to the paramount importance of understanding the fundamental physical and chemical mechanisms that govern colloidal fouling of membranes.

Recent studies have shown that membrane surface morphology and structure influence performance characteristics of membranes [1–9]. Hirose et al. [9] suggested an approximately linear relationship between membrane surface roughness and permeate flux for crosslinked aromatic polyamide reverse osmosis (RO) membranes, where permeability increased with increasing surface roughness. The linear relationship was attributed to surface unevenness of the RO membrane skin layer, which resulted in enlargement of the

* Corresponding author. Tel.: +1-203-432-2789; fax: +1-203-432-2881.
E-mail address: menachem.elimelech@yale.edu (M. Elimelech).

0376-7388/01/$ – see front matter
PII: S0376-7388(01)00376-3

effective membrane area. Kwak et al. [4] showed that substitution of bisphenol biphenyl rings with either methyl or halogen strongly influenced rejection and permeability of aromatic polyester RO membranes. Higher flux and lower rejection were associated with the smoother membrane surfaces obtained from methyl substitution, while lower flux and higher rejection were associated with the rougher membrane surfaces resulting from halogen substitution. Additional work by Kwak and Ihm [5] coupling nuclear magnetic resonance (NMR) spectroscopy and atomic force microscopy (AFM) has shown an important relationship between proton spin–lattice relaxation times and RO permeability, regardless of surface morphological features. The latter two studies suggest that membrane performance (flux and rejection) is strongly influenced by the structure of the polymer network which constitutes the thin-film active layer.

Several fundamental investigations of membrane fouling have explored the effects of membrane surface properties such as pore size and pore size distribution, surface roughness and structure, electrokinetic (zeta potential) characteristics, chemical properties (hydrophobic/hydrophilic), and specific chemical structure [1,3,6–8]. Various analytical techniques have been employed for elucidating specific physical and chemical surface properties of membranes, including Raman spectroscopy (structure) [1], electron spin resonance (solute mobility in membrane polymer matrix and pores) [1], AFM (surface morphology, structure, and pore size) [1–9], streaming potential (membrane surface zeta potential) [10,11], NMR spectroscopy (permeability) [5], contact angle [12], and X-ray photoelectron spectroscopy (XPS) for surface chemical functional groups [13,14]. Despite these efforts, however, the role of membrane surface properties in colloidal fouling of RO/NF membranes is still not well understood.

This investigation relates several key membrane surface properties of four commercial RO/NF membranes to their initial colloidal fouling behavior during crossflow membrane filtration. The aromatic polyamide thin-film composite membrane surfaces were characterized for morphological properties (AFM), contact angle, zeta potential, and specific chemical structure (XPS). Membrane fouling, determined by percent of flux decline for a specific volume of permeate filtered, was correlated to the measured membrane surface properties. It was demonstrated that colloidal fouling of the RO and NF membranes was strongly correlated only with membrane surface roughness. A novel mechanistic explanation for the striking effect of membrane surface roughness on colloidal fouling behavior is proposed.

2. Materials and methods

2.1. Membranes

Four commercial RO/NF thin-film composite membranes were used in this study. The RO membranes were Hydranautics LFC-1 (Oceanside, CA) and Trisep X-20 (Goleta, CA). The NF membranes were Dow-FilmTec NF-70 (Minneapolis, MN) and Osmonics HL (Minnetonka, MN). All membranes were stored in deionized (DI) water at 5°C with water replaced regularly. The membranes were characterized for intrinsic physical and chemical properties such as zeta potential, roughness (AFM), contact angle, chemical composition (XPS), and performance (pure water flux and salt rejection).

2.1.1. Membrane surface zeta potential

Membrane surface zeta potential was determined by a streaming potential analyzer (EKA, Brookhaven Instruments Corp., NY) following the procedure described by Childress and Elimelech [11]. Three runs on three separate days were performed for three different samples of each membrane at an ionic strength of 0.01 M NaCl and pH ranging from 3 to 9.

2.1.2. Membrane AFM analysis

Membrane surface roughness was determined by AFM imaging and analysis (Multi-Mode AFM, Digital Instruments, Santa Barbara, CA). Imaging was performed in tapping mode with an etched silicon probe (TESP, Digital Instruments, Santa Barbara, CA). The TESP probes had a spring constant of 20–100 N/m, resonant frequency of 200–400 kHz, nominal tip radius of 5–10 nm, and cantilever length of 160 μm. Clean membrane coupons were removed from storage in DI water and allowed to air dry before AFM scans were performed. Fouled membranes were removed from crossflow filtration devices following each experiment, and immediately rinsed in a

particle-free electrolyte solution similar to that used in the corresponding fouling experiment before air drying.

2.1.3. Membrane contact angle measurement

Contact angle measurements were obtained via a goniometer (Rame-Hart Inc., Mountain Lakes, NJ). Three equilibrium contact angles as described by Marmur [15] were measured for each membrane. Each equilibrium contact angle was the average of the left and right contact angles, and the reported values are the average of three equilibrium contact angles.

2.1.4. Membrane XPS analysis

All XPS analyses were performed using a 5400 PHI ESCA spectrometer (Physical Electronics, Eden Prarie, MN). A non-monochromated aluminum Kα X-ray source ($h\nu = 1486.6$ eV) at a power of 250 W was used for the analysis. Acceleration voltage was 15 kV and amperage was 12–18 mA. Spectral deconvolution was performed by first removing Shirley background and minimizing fit error using a standard peak-fit software. The second and fourth derivatives of the spectrum were inspected to locate the positions of various peaks. The core level peaks were then successfully fitted with component peaks with a Gaussian–Lorentzian distribution. It is important to note that the polyamide membrane specimens in this study were fully aromatic, and that the carbon C 1s was at a binding energy of 285 eV, not the adventitious carbon C 1s peak at 284.6 eV [16]. Peaks were placed according to positions found in literature, and full-width–half-max was fixed. This allowed the program to fit the amplitude of the peaks.

2.1.5. Membrane performance testing

Pure water flux and salt-rejection performance tests were performed in triplicate for each membrane. Membrane coupons were cut from flat sheet rolls and allowed to soak in DI water at room temperature for at least 30 min. Membranes were loaded into the test cells and DI water was filtered through the unit (and membrane) at a starting pressure of 1724 kPa (250 psi) for RO membranes or 1034 kPa (150 psi) for NF membranes. At least 2 l of permeate was wasted to ensure that preservatives or other chemicals coating the membrane were flushed out. DI water was then circulated through the unit for 24 h to allow the membranes to equilibrate and attain steady-state performance.

After a constant flux was achieved at the starting pressure, operating pressure was decreased in increments of 172 kPa (25 psi) down to 345 kPa (50 psi). At each pressure, flux was monitored for at least 60 minutes, or until a satisfactory steady state was achieved. When flux at 345 kPa was maintained steady for at least 30 min, an appropriate volume of premixed stock of NaCl solution was added to provide a 0.01 M (585 mg/l) salt concentration. After salt addition, the unit was allowed to equilibrate until a satisfactory steady-state flux was again reached. Permeate, retentate, and feed samples were drawn, and conductivity (YSI Inc., Yellow Springs, OH) and pH (Accumet 1500 pH Meter, Fisher Scientific, Pittsburgh, PA) were measured. Operating pressure was then increased in increments of 172 kPa (25 psi) with pH and conductivity measurements being made once steady-state flux was achieved at each pressure.

2.2. Colloidal particles

The colloidal particles used in the fouling experiments were provided by Nissan Chemical America Corporation (Houston, TX). The particles were certified as 0.10 μm (±0.03 μm) silica particles in an aqueous suspension. Chemical analysis by the manufacturer indicates the suspension to be 40.7 wt.% amorphous silica and below 0.08 wt.% Na_2O with a specific gravity of 1.3. Based on the specific gravity and weight percent of the suspension the particle density was calculated to be 2.36 g/cm^3. Gravimetric analysis of the particle suspension revealed the particle density to be 2.11 g/cm^3, which compares well with the above calculation and other reported values [17]. Model silica colloids were further characterized for size, shape, and zeta potential.

The size of colloidal silica used was determined by dynamic light scattering (Zeta PALS, Brookhaven Instruments Corp., NY). Size and shape of the particles were also verified by scanning electron microscope (SEM) imaging. The zeta potential of the colloidal silica was determined from electrophoretic mobility measurements (Zeta PALS, Brookhaven Instruments Corp., NY) using the tabulated data of Ottewill and Shaw [18]. The electrophoretic mobility measurements were performed at ionic strengths of 0.01 and

0.001 M NaCl and over a pH range of 2–10.

2.3. Standards and reagents

Salt stock solutions were prepared using ACS grade NaCl (Fisher Scientific, Pittsburgh, PA) dissolved in DI water (Nanopure Infinity Ultrapure, Barnstead, Dubuque, Iowa). ACS grade HCl and NaOH were used to make pH adjustments during membrane and particle zeta potential measurements.

2.4. Crossflow membrane filtration unit

The test apparatus shown in Fig. 1 was a modified version of a commercially available stainless steel crossflow membrane filtration (CFMF) unit (Sepa CF, Osmonics, Minneatonka, MN). The Sepa CF test unit is rated for operating pressures up to 6895 kPa (1000 psi) and has dimensions of channel length of 14.6 cm, channel width of 9.5 cm, and channel height of 1.73 mm. These channel dimensions provide an effective membrane area of $1.39 \times 10^{-2}\,m^2$ and a cross-sectional flow area of $1.64 \times 10^{-4}\,m^2$.

A 6.83 l/min (1.8 gpm) constant flow diaphragm pump (Hydracell, Wanner Engineering, Inc., Minneapolis, MN) delivered the feed suspension to the Sepa CF cell at a maximum pressure of 3447 kPa (500 psi). The feed suspension was fed from a magnetically stirred high-density polyethylene 20 l reservoir. Feed water temperature was maintained at a constant 25°C by a recirculating heater/chiller (RTE-111, Neslab, Portsmouth, NH).

Additional modifications to the original manufacturer's setup included the installation of a bypass needle valve (Swagelok, Solon, OH) before the channel inlet and a back-pressure regulator (US Paraplate Corp., Auburn, CA) at the channel outlet. The combination of the needle valve and back-pressure regulator allowed fine control over a wide range of applied pressures and crossflow velocities within the CFMF unit. Permeate flux was continuously measured by a digital flowmeter (Optiflow 1000, J&W Scientific Inc., Folsom, CA), and downloaded in real time to a PC. A floating disk rotameter (King Instruments, Fresno, CA) was installed after the back-pressure regulator to continuously monitor crossflow velocity.

2.5. Membrane fouling studies

Membrane coupons were cut from flat sheet membranes stored in DI water at 5°C. The membrane coupons were soaked in DI water at room temperature for at least 30 min prior to loading in the CFMF test unit. In order to dissociate any flux decline due to compaction (and other unknown causes inherent of lab-scale recirculation systems) from that due to colloidal fouling, the membrane was equilibrated before the fouling tests. Membrane equilibration was carried

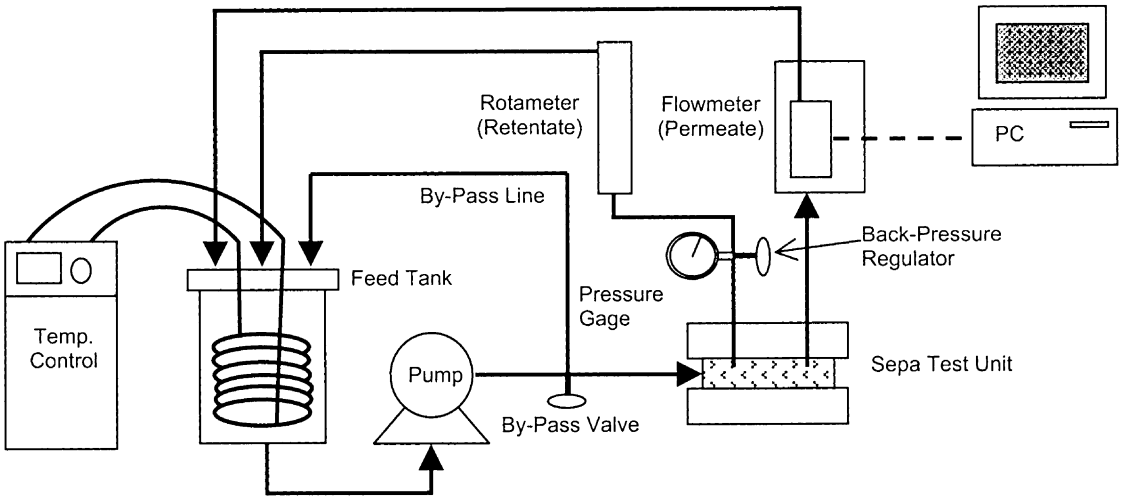

Fig. 1. Modified "Sepa CF" recirculating crossflow membrane-filtration apparatus used in colloidal fouling experiments.

out first by filtering 2 l of DI water (permeate wasted, retentate recycled), then equilibrating with DI water (permeate and retentate recycled) until a satisfactory steady state is achieved. The equilibration was conducted at an operating pressure of 1724 kPa (250 psi) for RO membranes and 1034 kPa (150 psi) for NF membranes, and typically lasted 24 h.

After equilibration, the pressure was adjusted to generate the pure water flux at which the fouling experiment would be started until steady state was observed. Then, a stock electrolyte solution was added to the feed tank to provide the appropriate background electrolyte (NaCl) concentration. The pressure was adjusted, as needed, to obtain the initial permeation rate of the fouling experiment, and the solution was circulated until a satisfactory steady state was achieved. The duration of this equilibration stage varied for each membrane, but typical electrolyte solution equilibration time was 4–6 h. Last, a dose of silica particles was added to the feed tank to provide a feed concentration of 200 mg/l (unless otherwise noted). The silica particles were sonicated in a heated (25°C) water bath ultrasonicator (Fisher Scientific FS60, Pittsburgh, PA) to ensure monodispersity prior to being added to the feed tank. Flux was monitored continuously for the duration of the experiment and recorded in real time on a laboratory computer. Conductivity, pH, and turbidity measurements were made at the start, end, and at several points during the fouling experiment to monitor salt rejection, and to ensure that the chemical conditions were constant throughout the test.

3. Results and discussion

3.1. Membrane fouling experiments

Several fouling experiments were performed to provide a basic understanding of the influence of physical and chemical operating (feed) conditions on colloidal fouling behavior of the test membranes. The effects of varying initial flux, ionic strength, and crossflow velocity (wall shear rate) were systematically investigated. The expected behavior for each condition was observed, whereby decreasing the initial flux or ionic strength or increasing the crossflow velocity (shear rate) significantly decreased fouling.

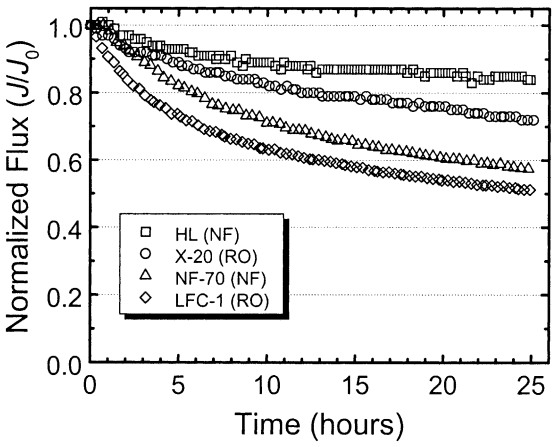

Fig. 2. Experimental flux decline (fouling) data for Osmonics HL (NF), Trisep X-20 (RO), Dow-FilmTec NF-70 (NF), and Hydranautics LFC-1 (RO) membranes. Test conditions employed were: initial flux (J_0) = 1.415×10^{-5} m/s (30 gfd), feed particle concentration (C_p) = 200 mg/l (0.009% (v/v)), ionic strength (I) = 50 mM NaCl, crossflow velocity (u_{XF}) = 0.096 m/s, shear rate (γ_0) = 324 s^{-1}, temperature = 25°C, and pH = 6.8 ± 0.2.

A significant difference in the rate and extent of fouling of each membrane is obvious when flux decline data are plotted versus time as shown in Fig. 2. The test conditions in these experiments were an initial flux (J_0) of 1.415×10^{-5} m/s (30 gfd), ionic strength (I) of 0.05 M NaCl, feed particle concentration (C_p) of 200 mg/l, crossflow velocity (u_{XF}) of 0.096 m/s, wall shear rate (γ_0) of 334 s^{-1}, temperature of 25°C, and pH of 6.8 (±0.2). When compared on the basis of percent flux decline for a given volume of permeate filtered (10 l), the membranes rank in the following order

$$\text{HL (13.9\%)} < \text{X-20 (38.3\%)} < \text{NF-70 (46.9\%)} < \text{LFC-1 (49.3\%)}$$

Experiments similar to those described in Fig. 2 were carried out at a lower ionic strength (0.01 M NaCl) and, as expected, the membranes fouled less at 0.01 M than at 0.05 M. However, when compared on the basis of percent flux decline for 10 L of permeate filtered, the membranes fouled in the same order:

$$\text{HL (13.4\%)} < \text{X-20 (21.8\%)} < \text{NF-70 (27.2\%)} < \text{LFC-1 (28.9\%)}$$

Increasing the crossflow velocity from 0.096 to 0.192 m/s (corresponding to shear rates of 334 and

$1336\,s^{-1}$, respectively) at an ionic strength of 0.01 M NaCl resulted in even less fouling. When compared on the basis of percent flux decline for 10 l of permeate filtered, the membranes fouled to varying extents, but again in the same order:

$$\text{HL (0.0\%)} < \text{X-20 (5.3\%)} < \text{NF-70 (8.0\%)} < \text{LFC-1 (9.3\%)}$$

Since varying electrolyte concentration (ionic strength) and crossflow velocity (shear rate) altered the extent of membrane fouling, but not the order in which these membranes fouled, it was concluded that some intrinsic properties of the membranes governed the fouling behavior.

3.2. Correlation of membrane surface properties with fouling behavior

The physical properties (surface morphology), chemical properties (zeta potential, contact angle, and elemental composition), and performance attributes (pure water permeability and salt rejection) of the four test membranes were investigated. The observed colloidal fouling behavior was related to these measured physical and chemical membrane properties to elucidate the key factors controlling colloidal fouling.

3.2.1. Correlation of membrane surface morphology with fouling data

The AFM images of the four membranes shown in Fig. 3 reveal different extents and occurrences of surface roughness. Note that the (horizontal) X and Y scales are $10\,\mu m \times 10\,\mu m$ ($2\,\mu m$/division), while the (vertical) Z-axis is $1.0\,\mu m$ (500 nm/division). This distorted scale increases peak-to-valley distances relative to peak-to-peak separation in the AFM images.

The key physical parameters obtained from the AFM analysis are correlated with the fouling data of each membrane in Table 1. The fouling data for the membranes, characterized as percent flux decline for 10 l of permeate volume filtered, was determined from the fouling curves in Fig. 2. The correlation coefficient ($\rho_{X,Y}$) for each physical membrane surface property and the percent flux decline measures the relationship (scaled to be independent of the unit of measurement) between the two data sets. For descriptive purposes, the relationship between two data sets is considered "strong" if $|\rho_{X,Y}| > 0.8$, "moderate" if $0.8 > |\rho_{X,Y}| > 0.5$, and "weak" if $|\rho_{X,Y}| < 0.5$ [19].

Mean plane (the arithmetic average of all height values obtained from the AFM analysis) is moderately positively correlated with flux decline data, but does not qualitatively predict the correct fouling trend. Another key physical parameter obtained from the AFM analysis is surface area difference, which gives the increase in surface area (due to roughness) over a perfectly flat plane with the same projected area. Surface area difference is weakly-to-moderately positively correlated with fouling. Peak count (the number of peaks in the area scanned) is weakly-to-moderately negatively correlated with membrane fouling. Average roughness is defined as the average deviation of the peaks and valleys from the mean plane, and root mean squared (RMS) roughness is the RMS deviation of the peaks and valleys from the mean plane. From the near perfect correlation between membrane roughness and the fouling data, it is obvious that membrane roughness is the most influential physical membrane surface property.

Table 1
Membrane physical properties determined by AFM correlated with the flux decline data of Fig. 2[a]

Membrane name (type)	Flux decline[b] J/J_0 (%)	Average roughness (nm)	RMS roughness (nm)	Surface area difference (%)	Peak count	Mean plane (nm)
HL (NF)	13.9	10.1	12.8	1.2	545	0.065
X-20 (RO)	38.3	33.4	41.6	32.7	859	0.049
NF-70 (NF)	46.9	43.3	56.5	20.7	210	0.121
LFC-1 (RO)	49.3	52.0	67.4	16.9	146	0.147
Correlation coefficient	–	0.99	0.98	0.67	−0.49	0.68

[a] Fouling test conditions: $J_0 = 1.415 \times 10^{-5}$ m/s (30 gfd), $I = 0.05$ M NaCl, $C_p = 200$ mg/l, $u_{XF} = 0.096$ m/s, and pH = 6.8.
[b] Percent flux decline determined for 10 l of permeate volume filtered.

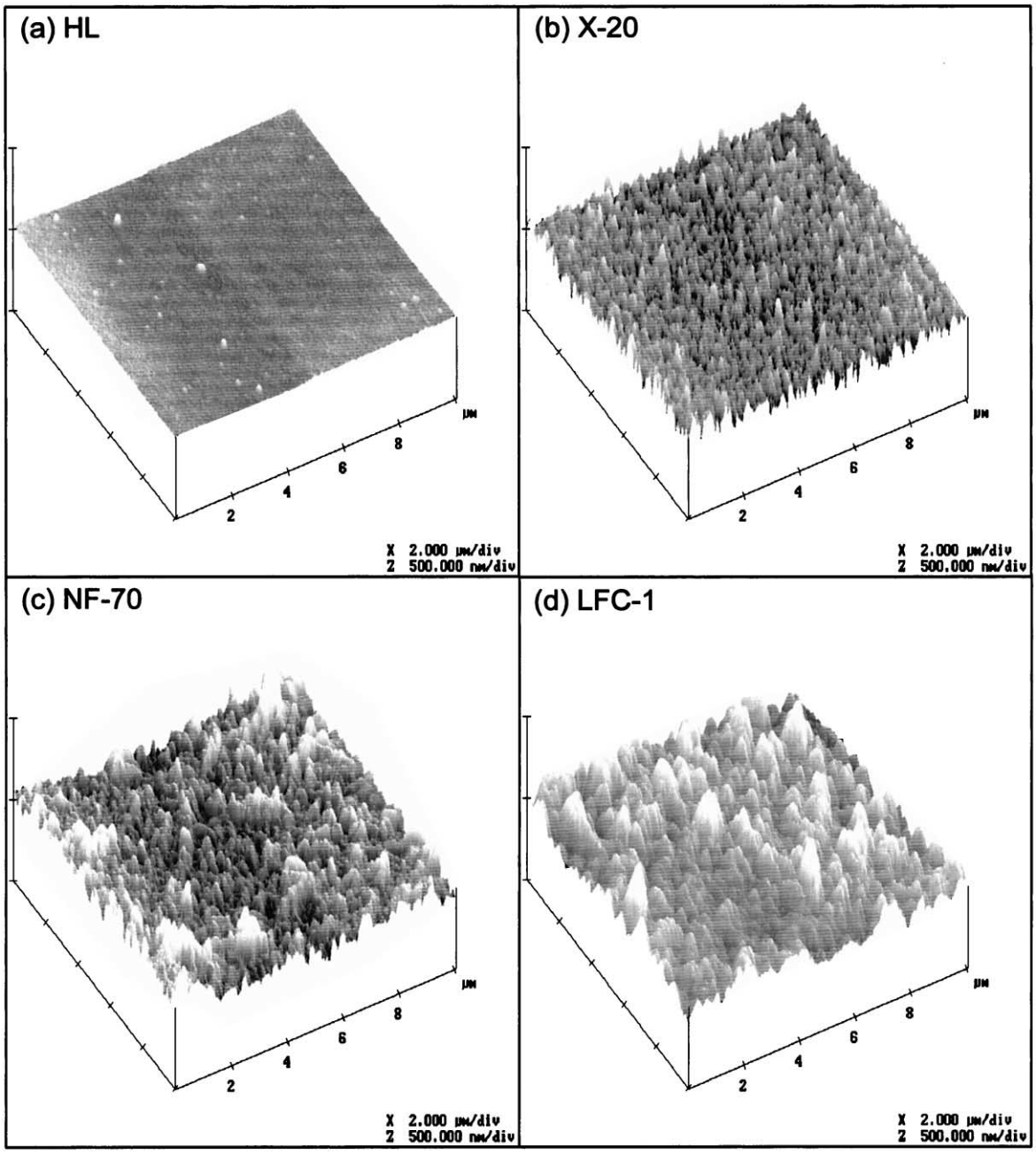

Fig. 3. AFM images of (a) Osmonics HL (NF); (b) Trisep X-20 (RO); (c) Dow-FilmTec NF-70 (NF); (d) Hydranautics LFC-1 (RO) membranes. Note that the *X* and *Y* dimensions are both 10 μm (2 μm/division), while the *Z*-scale is 1 μm (500 nm/division). Average roughness parameters calculated for each membrane were 10.1, 33.4, 43.3, and 52.0 nm for HL, X-20, NF-70, and LFC-1, respectively.

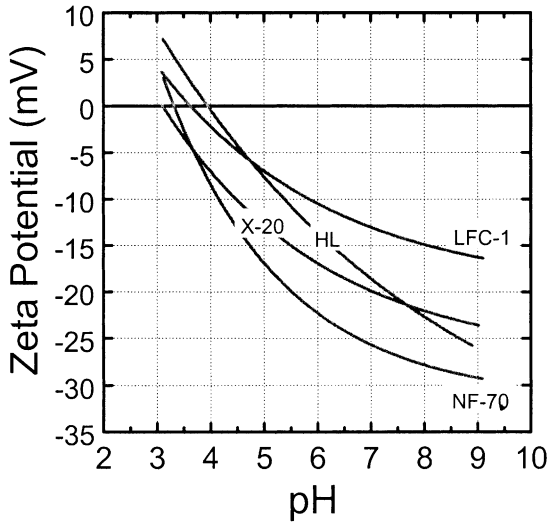

Fig. 4. Membrane surface zeta potential plotted as a function of solution pH, at a background electrolyte concentration of 0.01 M NaCl. The solid line curve for each membrane represents a polynomial fit for three sets of zeta potential vs. pH measurements conducted on separate days with different membrane samples. At the test conditions employed in most fouling experiments (0.01 M NaCl and pH 6.8 ± 0.2) the membrane surface zeta potentials were −13, −18, −20, and −25 mV for LFC-1, HL, X-20 and NF-70, respectively.

3.2.2. Correlation of physical and chemical membrane properties with fouling

In addition to AFM analysis, the four membranes were characterized for zeta potential, contact angle, pure water permeability, and observed salt (NaCl) rejection. The zeta potential versus pH curves for the four membranes are shown in Fig. 4. At the fouling test conditions, the membrane surface zeta potentials were −13, −18, −20, and −25 mV for LFC-1, HL, X-20, and NF-70, respectively. These values indicate that repulsive electrostatic double layer interactions would develop between the negatively charged silica particles and membrane surfaces during the fouling experiments. It is further expected that these repulsive electrostatic interactions are more significant for the more negatively charged membranes.

The key membrane physical, chemical, and performance properties are correlated with flux decline data in Table 2. Neither zeta potential nor contact angle was correlated with fouling behavior. Pure water permeability was weakly negatively correlated to fouling, whereas salt rejection was moderately-to-strongly positively correlated. The relatively high correlation of salt rejection to fouling is fortuitous since the smoothest membrane (HL) also has the lowest salt rejection. In direct contrast, LFC-1 and X-20 have exactly the same salt rejection, but their fouling behavior is clearly related to membrane roughness. Average membrane roughness values are shown again to emphasize the extremely strong correlation with fouling relative to the other membrane properties.

3.2.3. Correlation of membrane elemental composition with baseline fouling data

Additional investigation into membrane surface chemistry via XPS revealed weak-to-moderate correlations between total atomic percentages of carbon, nitrogen, oxygen, and sulfur, but no qualitatively correct predictive trend could be derived from the data shown in Table 3. The small atomic percents of sulfur groups observed for X-20 and LFC-1 may originate from unreacted sulfur pendants of the chemical

Table 2
Physical, chemical, and performance properties of the membranes and their correlation with flux decline (fouling) data[a]

Membrane name (type)	Flux decline[b] J/J_0 (%)	Average roughness (nm)	Zeta potential[c] (mV)	Contact angle (°)	Pure water permeability (10^{-12} m/Pa s)	Salt (NaCl) rejection[d] (%)
HL (NF)	0.00	10.1	−18.0	51.9	30.7	35.0
X-20 (RO)	5.32	33.4	−20.0	54.1	8.8	98.0
NF-70 (NF)	7.97	43.3	−25.0	51.7	31.9	83.0
LFC-1 (RO)	9.32	52.0	−13.0	52.5	11.0	98.0
Correlation coefficient	–	1.00	0.05	0.07	−0.41	0.87

[a] Fouling test conditions: $J_0 = 1.415 \times 10^{-5}$ m/s (30 gfd), $I = 0.01$ M NaCl, $C_p = 200$ mg/l, $u_{XF} = 0.192$ m/s, and pH = 6.8.
[b] Percent flux decline determined for 101 of permeate volume filtered.
[c] $I = 0.01$ M NaCl, pH = 6.8.
[d] $J_0 = 1.415 \times 10^{-5}$ m/s (30 gfd), $I = 0.01$ M NaCl, $u_{XF} = 0.192$ m/s, and pH = 6.8.

Table 3
XPS analyses correlating atomic percentages with flux decline data of Fig. 2[a]

Membrane name (type)	Flux decline[b] J/J_0 (%)	Average roughness (nm)	Total atomic percentages of C 1s (%)	Total atomic percentages of O 2s (%)	Total atomic percentages of N 1s (%)	Total atomic percentages of S 2p3 (%)
HL (NF)	13.9	10.1	91.9	4.60	3.40	0.00
X-20 (RO)	38.3	33.4	73.6	14.9	11.3	0.20
NF-70 (NF)	46.9	43.3	58.2	31.8	10.1	0.00
LFC-1 (RO)	49.3	52.0	90.6	8.00	1.30	0.10
Correlation coefficient	–	0.99	−0.47	0.54	0.21	0.32

[a] Fouling test conditions: $J_0 = 1.415 \times 10^{-5}$ m/s (30 gfd), $I = 0.05$ M NaCl, $C_p = 200$ mg/l, $u_{XF} = 0.096$ m/s, and pH = 6.8.
[b] Percent flux decline determined for 10 l of permeate volume filtered.

compounds used in interfacial polymerization [14]. It is also possible that XPS penetrates deeply enough in certain places (e.g. "valleys" of roughness) to detect small amounts of sulfur groups from the polysulfone support layer.

3.3. Additional membrane fouling studies correlated with membrane surface roughness

Flux decline data from several additional fouling experiments are correlated with membrane surface roughness in Table 4. The additional fouling experiments were performed to prove that the influence of membrane surface roughness on fouling was not limited to a specific set of physical and chemical operating conditions. The first three sets of fouling data were described in Section 3.1, with the differences in fouling behavior arising from changes in crossflow velocity and ionic strength. The first fouling data set is perfectly correlated with membrane surface roughness. The second and third columns of fouling data are nearly perfectly correlated with membrane surface roughness. The fourth data set is very highly correlated with membrane surface roughness although fouling was studied under totally different physical and chemical operating conditions. In this set of experiments, the initial flux, particle feed concentration, and crossflow velocity were all different from the previous three experiments. Furthermore, this fouling test was conducted in a crossflow membrane filtration device with different channel geometry (length-to-width and width-to-height aspect ratios). The altered channel geometry creates different Reynolds and Peclet numbers for similar crossflow velocities, and consequently, mass transport phenomena are quite different. Ultimately, the flux decline (fouling) data from Table 4 suggest that the fouling behavior of these membranes could be qualitatively predicted from membrane surface roughness measurements regardless of the physical or chemical test conditions employed.

Table 4
Correlation of flux decline data and average membrane surface roughness for systematically varied physical and chemical operating conditions

Membrane name (type)	Flux decline[a] J/J_0 (%)	Flux decline[b] J/J_0 (%)	Flux decline[c] J/J_0 (%)	Flux decline[d] J/J_0 (%)	Average roughness (nm)
HL (NF)	0.00	13.4	13.9	15.1	10.1
X-20 (RO)	5.32	21.8	38.3	19.4	33.4
NF-70 (NF)	7.97	27.2	46.9	21.4	43.3
LFC-1 (RO)	9.32	28.9	49.3	28.4	52.0
Correlation coefficient	1.00	0.99	0.99	0.93	–

[a] $J_0 = 1.415 \times 10^{-5}$ m/s (30 gfd), $C_p = 200$ mg/l, $I = 0.01$ M NaCl, $u_{XF} = 0.192$ m/s, and pH = 6.8.
[b] $J_0 = 1.415 \times 10^{-5}$ m/s (30 gfd), $C_p = 200$ mg/l, $I = 0.01$ M NaCl, $u_{XF} = 0.096$ m/s, and pH = 6.8.
[c] $J_0 = 1.415 \times 10^{-5}$ m/s (30 gfd), $C_p = 200$ mg/l, $I = 0.05$ M NaCl, $u_{XF} = 0.096$ m/s, and pH = 6.8.
[d] $J_0 = 9.433 \times 10^{-6}$ m/s (20 gfd), $C_p = 100$ mg/l, $I = 0.01$ M NaCl, $u_{XF} = 0.125$ m/s, and pH = 6.8.

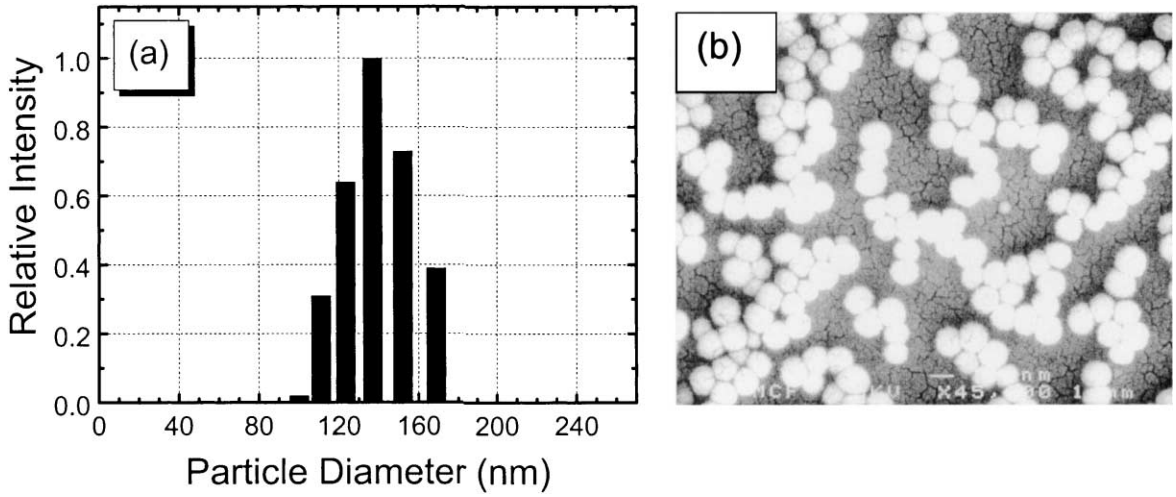

Fig. 5. Particle size and shape analysis from (a) dynamic light scattering measurements; (b) scanning electron microscopy.

3.4. Mechanistic explanation for the effect of roughness on initial rate of fouling

It is important to understand the physical and chemical properties of both the membranes and the model colloidal particles used in the fouling experiments to mechanistically explain the dominant influence of surface roughness on initial rate of fouling. The particle size distribution shown in Fig. 5(a) revealed a mean particle size of 140 nm. Model colloids were confirmed to be spherical and monodisperse by the SEM image in Fig. 5(b).

The zeta potential of the model colloids is plotted as a function of pH in Fig. 6 for 1 and 10 mM NaCl concentrations. The zeta potential behavior is comparable with previous studies of silica colloids [17,20]. At the pH and ionic strength of most of the fouling experiments (pH 6.8 ± 0.2, ionic strength 10 mM NaCl) the zeta potential of the colloids is approximately -25 mV, whereas the zeta potentials of the HL and NF-70 membranes are -18 and -25 mV, respectively. According to the classic Derjaguin–Landau–Verwey–Overbeek (DLVO) theory [21], the membrane with a more negative zeta potential would exhibit higher electrostatic double layer repulsion, and, therefore, be more fouling resistant to negatively charged colloids. However, our experimental fouling data consistently showed that NF-70 fouled more severely than HL.

One possible explanation for the lack of influence of membrane surface zeta potential is that the initial flux (1.415×10^{-5} m/s) used in the experiments was high enough that permeation drag forces completely overwhelmed electrostatic repulsive forces [7]. Additionally, the measured streaming potential used to calculate membrane surface zeta potential may not be appropriate for a crossflow device in which permeation through the membrane results in signifi-

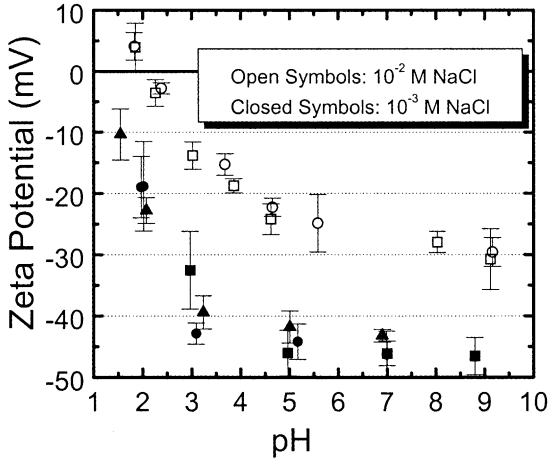

Fig. 6. Zeta potential behavior of the model silica colloids as a function of pH for ionic strengths of 1 mM NaCl (closed symbols) and 10 mM NaCl (open symbols). At the test conditions employed in most fouling experiments (0.01 M NaCl and pH 6.8 ± 0.2) the zeta potential of the model colloids was approximately -25 mV.

cant concentration polarization, and thus, elevated NaCl concentrations at the membrane surface. Regardless, it is concluded that the *relative* fouling behavior of the four commercial membranes can be qualitatively predicted from knowledge of surface roughness, but not from knowledge of zeta potential.

A mechanistic explanation for the pronounced influence of surface roughness on colloidal fouling emerges when analyzing the nature of membrane morphology and resistance, the limitations of AFM imaging, and the size of the model colloids. As permeation rate through RO/NF membranes is proportional to the thickness of the active (skin) layer, the thinnest section for water to permeate through a rough membrane will occur at the bottom of a "valley," with thickness increasing toward the peaks. Water will permeate through the entire surface of a rough membrane, but the bottom of a valley presents the "path-of-least resistance" to permeating water. Hence, water convection and particle transport are focused towards the valley bottom.

Another important aspect to consider is the actual geometry of the membrane surface morphology and the relative size of the colloidal particles. Due to the size of AFM scanning probe tips, there are some limitations to the depth to which a tip may penetrate a valley. It is suggested that the valleys of rough membranes may extend much deeper and even become narrower than AFM images are capable of depicting. Thus, as the 140 nm silica particles are preferentially convected towards the center of a valley they become wedged into the valley at the point that the valley constriction approaches the particle diameter. Because these "valleys" are likely to be of irregular shape (i.e. not necessarily round), a lodged particle may not completely "plug" the "pore-like" valley, but it may significantly restrict flow through the opening. Hence, the valleys rapidly become "clogged," resulting in significant loss of permeate flux.

By comparison, for a "smooth" membrane like HL, there will be no "valley clogging." Even if the same number of particles are deposited, they would likely be more evenly spaced (not focused into pore-like valleys) resulting in less overall flux decline (fouling). Based on the Carman–Kozeny equation [22], the resistance of a single layer of 140 nm particles to pure water permeation is more than a thousand times less than that of the clean membrane. This means that it would take a cake layer approximately 10 particle diameters thick to create roughly 1% permeate flux decline. Thus, for the smooth membrane, until a thick cake layer develops no flux decline will be detected. However, for a rough membrane, particles are preferentially transported into the valleys. The valleys quickly become clogged with multiple layers of densely packed particles increasing the cumulative resistance to flow in the valleys and leading to a more rapid loss of flux than for a smooth membrane.

To support the above hypothesis of "rapid valley clogging," several fouling experiments involving just the smooth (HL) and rough (NF-70) nanofiltration membranes were performed. A magnified view of representative initial fouling rate curves of HL and NF-70 is shown in Fig. 7. The conditions for this experiment were an initial flux (J_0) of 1.415×10^{-5} m/s (30 gfd), ionic strength (I) of 0.01 M NaCl, feed particle concentration (C_p) = 200 mg/l, crossflow velocity (u_{XF}) of 0.192 m/s, wall shear rate (γ_0) of $1334\,s^{-1}$, temperature of 25°C, and pH of 6.8 (±0.2). It is clear that HL did not foul at all, whereas NF-70 suffered a rapid loss of flux from the initial moments of the experiment. In fact, NF-70 continued to foul while HL showed no signs of flux decline for over 25 h. The lack of any flux decline indicates that these test conditions

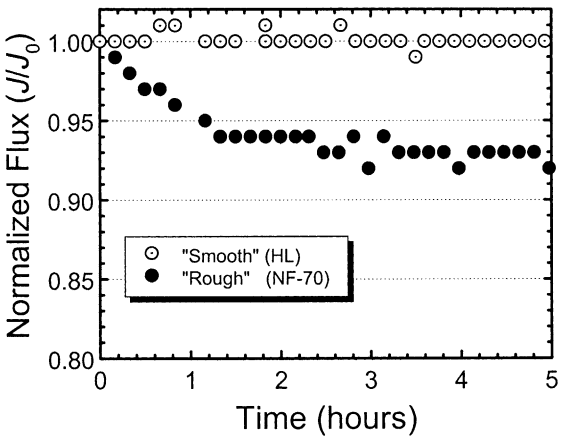

Fig. 7. Experimental flux decline (fouling) data comparing "smooth" HL and "rough" NF-70 nanofiltration membranes. Test conditions employed were: initial flux (J_0) = 1.415×10^{-5} m/s (30 gfd), feed particle concentration (C_p) = 200 mg/l (0.009% (v/v)), ionic strength (I) = 10 mM NaCl, crossflow velocity (u_{XF}) = 0.192 m/s, shear rate (γ_0) = $1334\,s^{-1}$, temperature = 25°C, and pH = 6.8 ± 0.2.

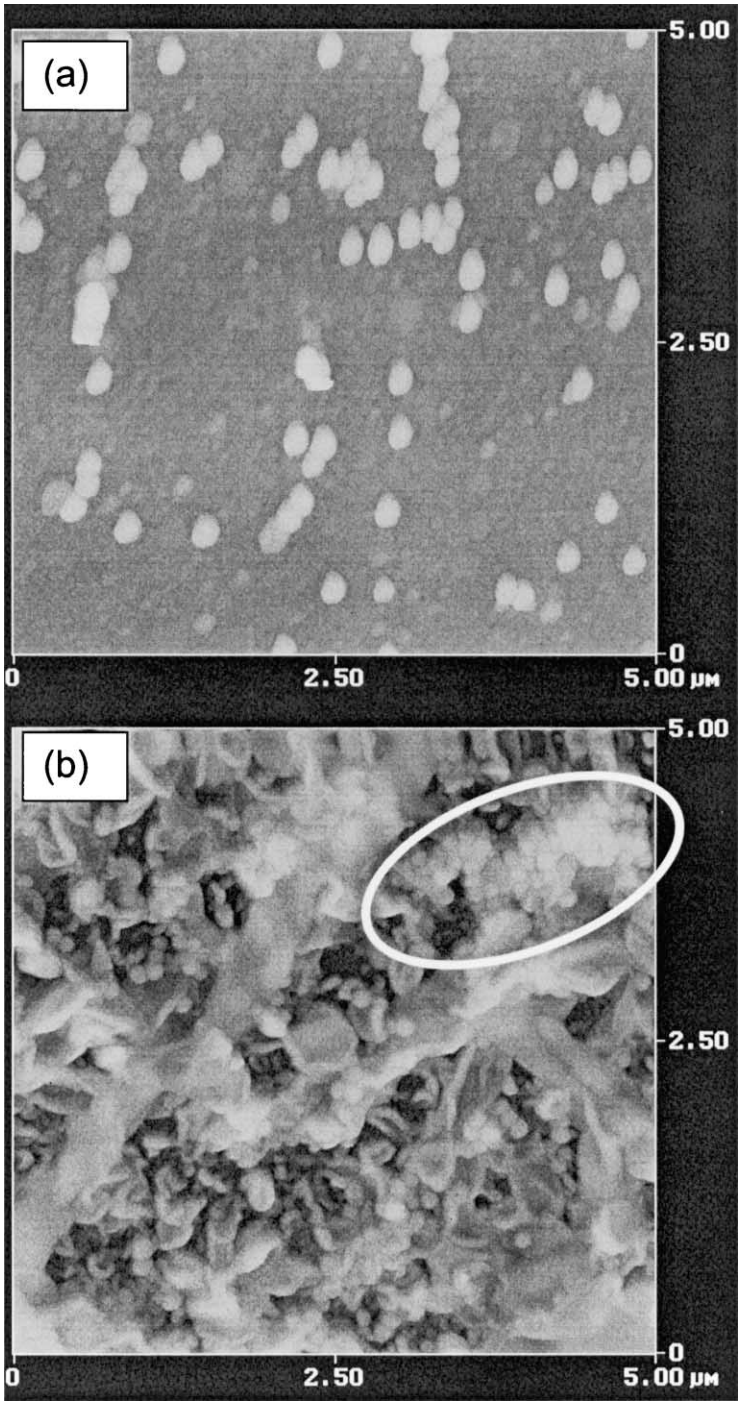

Fig. 8. Tapping mode AFM images of (a) HL, and (b) NF-70 nanofiltration membranes. Fouling test lasted for 30 s and test conditions were: initial flux (J_0) = 1.415×10^{-5} m/s (30 gfd), feed particle concentration (C_p) = 20 mg/l (0.0009% (v/v)), ionic strength (I) = 10 mM NaCl, crossflow velocity (u_{XF}) = 0.192 m/s, shear rate (γ_0) = 1334 s^{-1}, temperature = 25°C, and pH = 6.8 ± 0.2.

were at or below the "critical flux" conditions for the HL membrane.

A distinct difference in flux decline between the two membranes shown in Fig. 7 was measurable within the first 10 min of fouling. Therefore, several very short duration fouling experiments were coupled with AFM analysis to reveal the source of the different initial fouling behaviors. Test conditions were identical to those described in Fig. 2, but the fouling test lasted only for 60 s. Fouled membranes were examined by AFM and, while individual silica particles could be resolved, it was impossible to distinguish the cake layer thickness, as the membrane surface was not visible due to multilayer particle deposits.

More fouling experiments and AFM analyses were performed, in which ionic strength, particle feed concentration, and time of fouling were systematically reduced until evidence of less than a monolayer of deposited particles could be detected on the smooth HL membrane. The test conditions required to achieve this were particle feed concentration of 20 mg/l, ionic strength of 10 mM NaCl, and time of fouling limited to 30 s. The experiment was duplicated for HL, and AFM images were indistinguishable. The test was then performed twice for NF-70, and the fouled membranes were imaged by AFM.

The AFM image of HL revealed approximately 60–70 particles deposited on the 25 μm^2 scanned area shown in Fig. 8a. Both larger and smaller areas were scanned and revealed similar numbers of particles per unit area. The AFM images of NF-70, on the other hand, revealed clusters of densely packed particle deposits that were restricted to the valleys of the rough surface. In Fig. 8b there were well over 60 particles deposited in the valley in the upper right corner of the image (circled area). Additional particle clusters can be seen in other valley regions of NF-70. These AFM images provide visual verification of our hypothesis; i.e. particles are specifically attracted to the valleys of rough membranes during the initial stages of fouling, which results in "valley clogging" and leads to more rapid flux decline.

4. Conclusion

Laboratory-scale experiments were conducted to investigate the role of membrane surface properties on the initial rate of RO/NF membrane colloidal fouling. Membranes were characterized for key physical and chemical surface properties, and those properties were correlated with fouling data. In all cases, regardless of physical and chemical operating conditions, the rate and extent of colloidal fouling was most significantly influenced by the physical roughness of membrane surfaces. It was further demonstrated through use of AFM analysis that more particles deposit on rough membranes than on smooth membranes when all test conditions are held constant. AFM images revealed that particles preferentially accumulate in the valleys of rough membranes, leading to "valley clogging" and causing more severe flux decline than in smooth membranes.

Acknowledgements

The authors thank the American Water Works Association Research Foundation for supporting this project through Project No. 2514. The authors would also like to thank Dr. Amy Childress of the University of Nevada, Reno for performing the contact angle measurements; Hydranautics, Dow-FilmTec, Trisep, and Osmonics for supplying membranes; and Nissan Chemical America Corp. for providing the colloidal silica particles.

References

[1] K.C. Khulbe, T. Matsuura, Characterization of synthetic membranes by Raman spectroscopy, electron spin resonance and atomic force microscopy: a review, Polymer 41 (2000) 1917–1935.
[2] J.Y. Kim, H.K. Lee, S.C. Kim, Surface structure and phase separation mechanism of polysulfone membranes by atomic force microscopy, J. Membr. Sci. 163 (1999) 159–166.
[3] T. Knoell, J. Safarik, T. Cormack, R. Riley, S.W. Lin, H. Ridgway, Biofouling potentials of microporous polysulfone membranes containing a sulfonated polyether-ether-sulfone/polyethersulfone block copolymer: correlation of membrane surface properties with bacterial attachment, J. Membr. Sci. 157 (1999) 117–138.
[4] S.Y. Kwak, M.O. Yeom, I.J. Roh, D.Y. Kim, J.J. Kim, Correlations of chemical structure, atomic force microscopy (AFM) morphology, and reverse osmosis (RO) characteristics in aromatic polyester high-flux RO membranes, J. Membr. Sci. 132 (1997) 183–191.
[5] S.Y. Kwak, D.W. Ihm, Use of atomic force microscopy and solid-state NMR spectroscopy to characterize structure-

property-performance correlation in high-flux reverse osmosis (RO) membranes, J. Membr. Sci. 158 (1999) 143–153.
[6] K. Riedl, B. Girard, R.W. Lencki, Influence of membrane structure on fouling layer morphology during apple juice clarification, J. Membr. Sci. 139 (1998) 155–166.
[7] X. Zhu, M. Elimelech, Colloidal fouling of reverse osmosis membranes: measurements and fouling mechanisms, Environ. Sci. Technol. 31 (1997) 3654–3662.
[8] M. Elimelech, X. Zhu, A.E. Childress, S. Hong, Role of membrane surface morphology in colloidal fouling of cellulose acetate and composite aromatic polyamide reverse osmosis membranes, J. Membr. Sci. 127 (1997) 101–109.
[9] M. Hirose, H. Ito, Y. Kamiyama, Effect of skin layer surface structures on the flux behaviour of RO membranes, J. Membr. Sci. 121 (1996) 209–215.
[10] A.E. Childress, M. Elimelech, Relating nanofiltration membrane performance to membrane charge (electrokinetic) characteristics, Environ. Sci. Technol. 34 (2000) 3710–3716.
[11] A.E. Childress, M. Elimelech, Effect of solution chemistry on the surface charge of polymeric reverse osmosis and nanofiltration membranes, J. Membr. Sci. 119 (1996) 253–268.
[12] C. Combe, E. Molis, P. Lucas, R. Riley, M.M. Clark, The effect of CA membrane properties on adsorptive fouling by humic acid, J. Membr. Sci. 154 (1999) 73–87.
[13] E. Ferjani, M. Mejdoub, M.S. Roudesli, M.M. Chehimi, D. Picard, M. Delamar, XPS characterization of poly(methylhydrosiloxane)-modified cellulose diacetate membranes, J. Membr. Sci. 165 (2000) 125–133.
[14] S. Beverly, S. Seal, S. Hong, Identification of surface chemical functional groups correlated to failure of reverse osmosis polymeric membranes, J. Vac. Sci. Technol. A 18 (2000) 1107–1113.
[15] A. Marmur, Equilibrium contact angles: theory and measurement, Colloid Surf. A 116 (1996) 55–61.
[16] G. Beamson, D. Briggs, High Resolution XPS of Organic Polymers, Wiley, New York, 1992, p. 306.
[17] R.S. Faibish, M. Elimelech, Y. Cohen, Effect of interparticle electrostatic double layer interactions on permeate flux decline in crossflow membrane filtration of colloidal suspensions: An experimental investigation, J. Colloid Interface Sci. 204 (1998) 77–86.
[18] R.H. Ottewill, J.N. Shaw, Electrophoretic studies on polystyrene latices, J. Electroanal. Chem. 37 (1972) 133–143.
[19] J.L. Devore, Probability and Statistics for Engineering and the Sciences, 3rd Edition, Brooks/Cole Publishing, Pacific Grove, CA, 1991, p. 716.
[20] S. Hong, R.S. Faibish, M. Elimelech, Kinetics of permeate flux decline in crossflow membrane filtration of colloidal suspensions, J. Colloid Interface Sci. 196 (1997) 267–277.
[21] E.J.W. Verwey, J.T.G. Overbeek, Theory of the Stability of Lyophobic Colloids, Elsevier, Amsterdam, 1948, p. 218.
[22] R.H. Davis, Modeling of Fouling of Cross-Flow Microfiltration Membranes, Sep. Purif. Methods 21 (1992) 75–126.